

## Discovery and Validation of a Series of Aryl Sulfonamides as Selective Inhibitors of Tissue-Nonspecific Alkaline Phosphatase (TNAP)

Russell Dahl,<sup>†</sup> Eduard A. Sergienko,<sup>†</sup> Ying Su,<sup>†</sup> Yalda S. Mostofi,<sup>†</sup> Li Yang,<sup>†</sup> Ana Maria Simao,<sup>‡</sup> Sonoko Narisawa,<sup>‡</sup> Brock Brown,<sup>†</sup> Arianna Mangravita-Novo,<sup>†</sup> Michael Vicchiarelli,<sup>†</sup> Layton H. Smith,<sup>†</sup> W. Charles O'Neill,<sup>§</sup> José Luis Millán,<sup>‡</sup> and Nicholas D. P. Cosford<sup>\*,†</sup>

<sup>†</sup>Conrad Prebys Center for Chemical Genomics and <sup>‡</sup>Sanford Children's Health Research Center, Burnham Institute for Medical Research, 10901 North Torrey Pines Road, La Jolla, California 92037, and <sup>§</sup>Renal Division, Department of Medicine, Emory University School of Medicine, Atlanta, Georgia 30322

Received March 27, 2009

We report the characterization and optimization of drug-like small molecule inhibitors of tissue-nonspecific alkaline phosphatase (TNAP), an enzyme critical for the regulation of extracellular matrix calcification during bone formation and growth. High-throughput screening (HTS) of a small molecule library led to the identification of arylsulfonamides as potent and selective inhibitors of TNAP. Critical structural requirements for activity were determined, and the compounds were subsequently profiled for in vitro activity and bioavailability parameters including metabolic stability and permeability. The plasma levels following subcutaneous administration of a member of the lead series in rat was determined, demonstrating the potential of these TNAP inhibitors as systemically active therapeutic agents to target various diseases involving soft tissue calcification. A representative member of the series was also characterized in mechanistic and kinetic studies.

### Introduction

Among the human alkaline phosphatases, tissue-nonspecific alkaline phosphatase (TNAP<sup>a</sup>) is essential for bone matrix mineralization.<sup>1</sup> The biological function of TNAP is to hydrolyze extracellular inorganic pyrophosphate (ePP<sub>i</sub>), an inhibitor of calcification, to maintain the correct ratio of P<sub>i</sub>/ePP<sub>i</sub> in skeletal tissues to enable normal skeletal calcification.<sup>2–4</sup> Elsewhere in the body, high ePP<sub>i</sub> levels prevent ectopic calcification.<sup>5</sup> In turn, low levels of ePP<sub>i</sub> have been associated with the development of soft-tissue calcification.<sup>6</sup> This deficiency of ePP<sub>i</sub> can be attributed to deficits in either the production or transport of pyrophosphate, as seen in *Enpp1* and *Ank* deficiencies.<sup>2,3</sup> This physiological state can result in rather severe clinical indications including idiopathic infantile arterial calcification (IIAC), ectopic ossification in spinal ligaments, ankylosis, and osteoarthritis.<sup>2–6</sup> Arterial calcification, particularly medial calcification aka Monckeberg's sclerosis, is a serious complication of chronic kidney disease, obesity, diabetes, and aging.<sup>7</sup> We have recently observed an

upregulation of TNAP in *Enpp1*<sup>−/−</sup> and *ank/ank* vascular smooth muscle cells (VSMC) and also in uremic aortas, suggesting that it is an important cause of ePP<sub>i</sub> deficiency and medial calcification and a potential therapeutic target.<sup>8,9</sup> Thus, an effort to find selective and potent small molecule inhibitors of TNAP as potential therapeutics is warranted. Herein we describe the discovery of potent small molecule TNAP inhibitors that, on systemic administration, are likely to cause a reduction in TNAP activity, resulting in an increase in the local amount of ePP<sub>i</sub> to prevent or ameliorate vascular calcification.

TNAP, as with all mammalian APs, has been shown to be inhibited by a limited number of small molecule compounds including L-homoarginine, levamisole, and theophylline (Figure 1).<sup>1,10</sup> However, these known inhibitors of TNAP are very weak binders and do not show specificity for the TNAP isozyme. In addition, they are not particularly effective at inhibiting the pyrophosphatase activity of TNAP. We previously reported the results of an initial high-throughput screening (HTS) campaign that led to the identification of several low micromolar inhibitors of TNAP.<sup>8</sup> We also reported the results of a second HTS campaign, performed within the Molecular Library Screening Center Network (MLSCN), which led to the discovery of several small molecule TNAP inhibitors with different mechanisms of action (MOA).<sup>11</sup> Subsequent work on the optimization of one of the series discovered in this recent HTS campaign culminated in the development of selective competitive pyrazole TNAP inhibitors with low nanomolar potency (Figure 1).<sup>12</sup> We now report the structure–activity relationship (SAR) studies and validation of a novel class of sulfonamides that are uncompetitive TNAP inhibitors showing excellent phosphatase

\*To whom correspondence should be addressed. Phone: (858) 646-3100. Fax: (858)- 646-3199. E-mail: ncosford@burnham.org.

<sup>a</sup> Abbreviations: AP, alkaline phosphatase; IAP, intestinal alkaline phosphatase; PLAP, placental alkaline phosphatase; TNAP, tissue-nonspecific alkaline phosphatase; IIAC, idiopathic infantile arterial calcification; VSMC, vascular smooth muscle cells; HTS, high-throughput screening; ADME, absorption, distribution, metabolism, excretion; CYP2C19, cytochrome P450 2C19; MLSCN, Molecular Libraries Screening Center Network; MLSMR, Molecular Libraries Small Molecule Repository; SAR, structure–activity relationship; MOA, mechanism of action; CDP-star, disodium 2-chloro-5-(5'-chloro-4-methoxy-4-methoxy-1,2-dioxetane-3,2'-tricyclo[3.3.1.1.3,7]decan-4-yl)-phenol-1-(dihydrogen phosphate); PAMPA, parallel artificial membrane permeability assay.

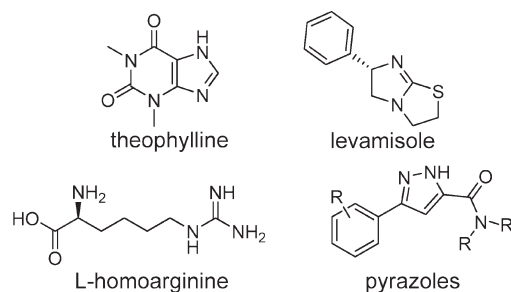


**Figure 1.** Structures of reported TNAP inhibitors.

selectivity and acceptable plasma levels in rat following subcutaneous administration. These compounds have the potential to be developed into therapeutic agents to treat vascular calcification.

## Results and Discussion

High-throughput screening (HTS) of 66000 compounds from the NIH Molecular Libraries Small Molecule Repository (MLSMR) compound collection (<http://www.mli.nih.gov/mlsmr>) using a luminescence-based HTS assay was performed as a part of the MLSCN initiative. These screening efforts led to the identification of several classes of submicromolar inhibitors of TNAP<sup>11</sup> (for assay details see Experimental Section and PubChem link to AID 1056 <http://pubchem.ncbi.nlm.nih.gov/assay/assay.cgi?aid=1056>). Initial HTS was performed at a concentration of 20  $\mu$ M and was followed with dose–response assays performed in duplicate using a 10-point 2-fold serial dilution of the hit compounds in DMSO. Hit confirmation was performed using luminescent and colorimetric assays to verify inhibitory activity against TNAP in dose–response mode. Selectivity was assessed against the isozymes placental and intestinal alkaline phosphatase (PLAP and IAP) in luminescence-based assays. Compounds that were active in dose–response mode against TNAP, soluble in the range relevant to their potency, and inactive against PLAP and IAP were prioritized for synthetic chemistry follow-up.

HTS hits and purchased commercial analogues provided an initial set of arylsulfonamides having TNAP  $IC_{50}$  values in the nanomolar to low micromolar range (Table 1). Interestingly, several compounds sharing similar structural features were also found that had greatly reduced activities compared to the initial lead structures, affording relevant information about the key required structural elements (Figure 2). Analysis of the nascent structure–activity relationship (SAR) present in those analogues showing confirmed activity revealed key features attributable to their inhibitory activity. Most notable was the presence of either 3-pyridyl or 3-quinoline moieties on the amine portion of the molecules and *ortho*-alkoxy substitution of the arylsulfonyl portion, which seemed to be required for activity. Additional substitution of methyl or halogen on this portion was equally tolerated in the active inhibitors. Finally, quinoline derivatives appeared to be more active than the corresponding pyridine analogues, as can be seen in the comparison of compounds **1** and **2** (Table 1).

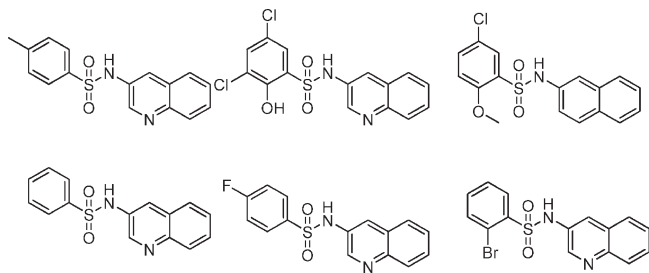
On the basis of the superior activity of compound **1**, a directed set of compounds was prepared to specifically address the key SAR requirements of this scaffold (Figure 3). It is noteworthy that when the two previously described SAR requirements were altered, the activity of the resulting derivatives was greatly diminished. Removal (**12**) or movement (**13**) of the quinoline nitrogen resulted in loss of activity. Replacement (**14**) or

**Table 1.** SAR of TNAP Inhibitors from HTS and Purchased Analogues

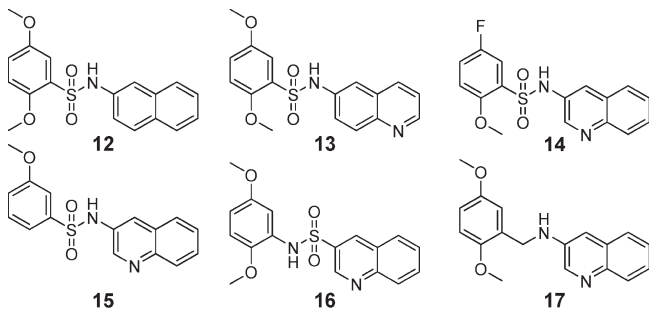
CMPD	TNAP $IC_{50}$ $\mu$ M luminescent <sup>a</sup>
	0.19 (0.03, 0.41, 43)
	1.06 (0.76, 1.48, 6)
	0.51 (0.28, 0.66, 3)
	0.54 (0.35, 0.65, 4)
	0.69 (0.24, 1.01, 6)
	1.13 (0.53, 1.93, 4)
	1.13 (0.49, 1.46, 4)
	1.29 (0.73, 1.56, 4)
	1.49 (0.64, 2.35, 3)
	1.55 (1.27, 1.83, 2)
	1.68 (1.07, 2.13, 3)

<sup>a</sup> TNAP  $IC_{50}$  data are presented as the geometric mean followed in parentheses by the lower and upper limits of the mean and the number of replicates.

movement of the 5-methoxy substituent of **1** also gave a similar reduction of activity. Next, removal of the *ortho*-methoxy (**15**) also resulted in a dramatic loss of activity. Finally, reversing the sulfonamide moiety (**16**) or replacement with an amide or methylene (**17**) also abolished the inhibitory activity. These analogues confirmed the key attributes of our lead series, specifically a 3-substituted quinoline or pyridine ring and an *ortho* alkoxy substituent on the arylsulfonyl ring.



**Figure 2.** Examples of inactive arylsulfonamides which gave insight into required structural elements. TNAP  $IC_{50} > 10 \mu M$  for all examples.

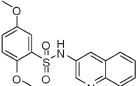
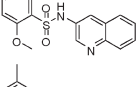
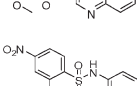
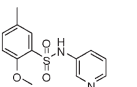
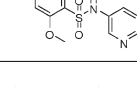
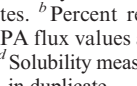


**Figure 3.** Elucidation of key requirements of lead TNAP inhibitor 1. TNAP  $IC_{50} > 10 \mu M$  for compounds 12–17.

After establishing the key features required for activity, additional analogues were prepared to further optimize the activity of this series and allow for in vitro profiling of absorption, distribution, metabolism, and excretion (ADME) properties. A variety of representative compounds showed activity in the high nanomolar to single-digit micromolar range. Notably, one analogue (**18**) possessed comparable activity to lead compound **1** (Table 2).

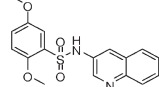
In addition, the compounds in Table 2 were profiled in in vitro ADME assays to assess their drug-likeness and potential for systemic activity in animal models of vascular calcification. Many of the sulfonamide compounds were shown to have suitable properties for oral administration including acceptable metabolic and plasma stability, good permeability across artificial lipid membranes, and good solubility. The results of the specific ADME profiling assays are shown in Table 2. Although the profiles of all of the synthesized analogues had acceptable and drug-like ADME profiles, it was clear that in addition to showing acceptable aqueous solubility at physiological pH, the overall properties of **1** were superior. The selectivity of **1** against other phosphatases and across other biological targets was remarkable (Table 3). TNAP inhibitor **1** showed no inhibition in over 250 assays reported in the PubChem database (<http://pubchem.ncbi.nlm.nih.gov/>) as well as assays performed in-house for two other alkaline phosphatase isozymes, intestinal alkaline phosphatase (IAP), and placental alkaline phosphatase (PLAP). Compound **1** showed activity in only one other assay, cytochrome P450 2C19 (CYP2C19). Compound **1** was also tested for its ability to inhibit the function of NPP1, a phosphodiesterase that also has phosphatase activity and regulates ePPI production in skeletal tissue,<sup>2,3</sup> and PHOSPHO1, a phosphatase with specificity for phosphethanolamine and phosphocholine, also involved in skeletal mineralization.<sup>13</sup> At their optimal alkaline pHs, inhibition was less than 9.5% for NPP1 and 7.4% for PHOSPHO1. Thus, TNAP inhibitor **1** was

**Table 2.** SAR and ADME Profiles of Follow-up Compounds of Lead TNAP Inhibitor **1**

CMPD	TNAP $IC_{50}$ $\mu M$ luminescent <sup>a</sup>	Microsomal/ Plasma Stability <sup>b</sup>	PAMPA (% FLUX) <sup>c</sup>	Solubility ( $\mu g/mL$ ) <sup>d</sup>
 <b>1</b>	0.19 (0.03, 0.41, 43)	78 / 97	58	138.2
 <b>18</b>	0.12 (0.04, 0.25, 16)	49 / 66	54	37.9
 <b>19</b>	0.65 (0.50, 0.94, 4)	48 / 91	7	71.6
 <b>20</b>	0.74 (0.74, 0.74, 1)	56 / 96	11	178
 <b>21</b>	1.85 (0.69, 3.36, 23)	39 / 98	83	28.5
 <b>22</b>	3.16 (2.27, 3.64, 4)	68 / 99	51	1.1

<sup>a</sup> TNAP  $IC_{50}$  data are presented as the geometric mean followed in parentheses by the lower and upper limits of the mean and the number of replicates. <sup>b</sup> Percent remaining after incubation for 30 min at 37 °C. <sup>c</sup> PAMPA flux values assessed according to previously published methods.<sup>15</sup> <sup>d</sup> Solubility measurements performed in an aqueous buffer solution at pH 7.4, in duplicate.

**Table 3.** Selectivity Profile of TNAP Inhibitor **1**

	Selectivity ( $IC_{50}$ , $\mu M$ )			PubChem (# of Assays)	
	TNAP	PLAP	IAP	Active	Inactive
	0.19	>100	>100	<b>2</b> (TNAP, CYP2C19)	258
PubChem CID 2931238					

established as a drug-like and selective probe molecule, prompting further evaluation of its therapeutic potential as a systemically active TNAP inhibitor.

The in vitro profile of **1** suggested that this compound had the potential for further development because it had properties indicative of systemic availability. To evaluate the potential for systemic activity, the plasma levels of compound **1** were assessed following subcutaneous administration. Rats were dosed subcutaneously with compound **1** at 4.13 mg/kg. At the 1 h time point, compound **1** showed plasma levels consistent with achieving therapeutic concentrations ( $C_{max} = 1.5 \mu g/mL$ ), indicating the potential for in vivo efficacy. In summary, these data indicate that compound **1** may find utility as an in vivo tool for elucidating the role of TNAP in vascular calcification in animal models.

### Mechanistic Studies

The mechanism of a general alkaline phosphatase reaction is outlined in Figure 4. Briefly, the initial alkaline phosphatase (E) catalyzed reaction consists of a substrate (DO-P<sub>i</sub>) binding step, phosphate-moiety transfer to Ser-93 (in the TNAP sequence of its active site), and product alcohol (DOH) release. In the second step of the reaction, phosphate is released through hydrolysis of the covalent intermediate (E-P<sub>i</sub>) and the noncovalent complex (E·P<sub>i</sub>) of the inorganic

phosphate in the active site. Phosphate release is the rate-limiting step of the overall reaction, resulting in accumulation of the phosphorylated enzyme. In the presence of nitrogen-containing alcohol molecules (AOH), such as the buffer diethanolamine (DEA), phosphate is also released via a faster transphosphorylation reaction without affecting the rate-limiting step. The physiological relevance and identity of the phosphate-acceptor molecules *in vivo* are not yet known.

To test the reversibility of binding of **1** to TNAP and to qualitatively estimate the rate at which equilibrium was achieved, the compound was serially diluted and preincubated with TNAP at a concentration 12.5-fold higher than in the final assay. Incubation at higher concentrations of a mixture of enzyme and inhibitor is a standard method to accelerate the binding process compared to the assay at normal concentrations. The rate of binding is proportional to the concentration

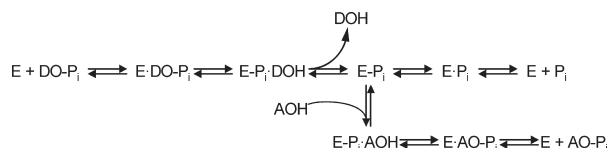
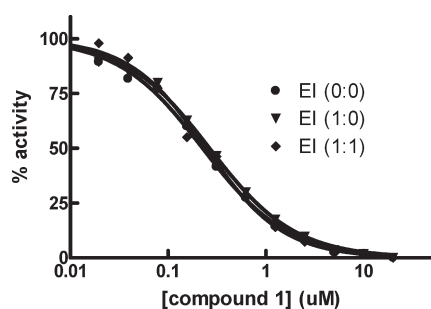


**Figure 4.** Catalytic mechanism of the alkaline phosphatase reaction. See text for details.



	EI (0:0)	EI (1:0)	EI (1:1)
IC <sub>50</sub> (uM)	0.23 ± 0.01	0.27 ± 0.01	0.24 ± 0.01
n <sub>H</sub>	1.00 ± 0.03	0.99 ± 0.03	1.09 ± 0.06

**Figure 5.** Time-dependent mechanistic studies of TNAP inhibition with **1**. The enzyme was added with compound **1** serially diluted immediately prior to activity measurement (●, EI (0:0)) or preincubated with the compound for 1 h at 12.5-fold of the concentrations and then diluted to final concentrations with (◆, EI (1:1)) or without (▼, EI (1:0)) an additional 1 h incubation after the dilution and prior to activity measurement. The dose-response curves were analyzed using the Hill equation; best-fit parameters (IC<sub>50</sub> and Hill coefficient *n<sub>H</sub>*) and their standard errors of fit are shown in the Table.

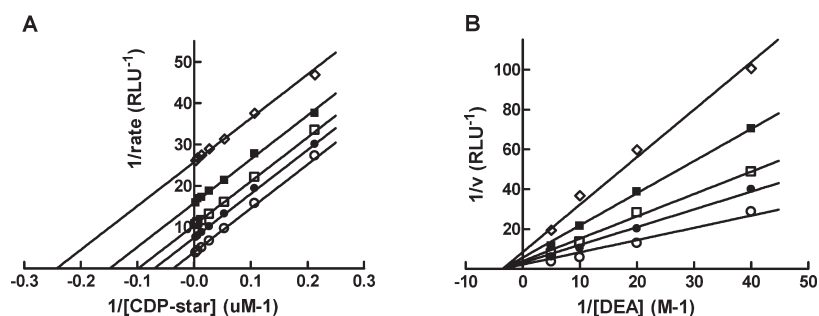


**Figure 6.** Lineweaver-Burk plots for compound **1** MOA experiments. Inhibition of TNAP was measured in the presence of the following concentrations of **1**: 0 μM (○), 0.195 μM (●), 0.39 μM (□), 0.78 μM (■), 1.56 μM (◇). The concentrations of DEA and CDP-star were equal to 100 mM (A) and 50 μM (B), respectively. The *K<sub>i</sub>* values for compound **1** are 0.34 μM (Figure 6A) and 0.59 μM (Figure 6B).

of reactants, an important consideration if the enzyme is inactivated through a collision-based mechanism by the compound itself or a product of its degradation. In addition, higher concentrations of inhibitor shifts the equilibrium of binding toward higher saturation within the enzyme-inhibitor complex, promoting any slow conversion of the enzyme-inhibitor complex.

The data for mechanistic experiments performed with TNAP inhibitor **1** are summarized in Figure 5. The binding of the compound appears to obey fast-equilibrium kinetics and lacks any time-dependent component. Compound potency in the assay was unchanged either right after mixing with the enzyme (EI 0:0) or after a preincubation for 1 h in the presence of elevated concentrations of compound **1** with (EI 1:1) or without (EI 1:0) an additional 1 h incubation post-dilution to the final compound concentrations.

In addition, we completed detailed mechanism of action (MOA) studies with **1** at different concentrations of phosphate-donor substrate, 1,2-dioxetane reagent disodium 2-chloro-5-(5'-chloro-4-methoxyspiro[1,2-dioxetane-3,2'-tricyclo[3.3.1.1.3,7]decan]-4-yl)-phenol-1-(dihydrogen phosphate) (CDP-star), or phosphate-acceptor substrate, diethanolamine (DEA). Defining the binding mode and site of action is important for building a predictive pharmacophore model to facilitate future medicinal chemistry efforts. The artificial substrate CDP-star is expected to provide an adequate system for studying the effects of compound **1** on TNAP because the rate-limiting step for the reaction is downstream of active site phosphorylation, as noted previously. As shown in Figure 6A, [CDP-star]-dependent curves obtained in the presence of different concentrations of **1** and plotted using Lineweaver-Burk coordinates yields parallel lines. This confirms the uncompetitive nature of the compound binding versus the CDP-star substrate arising from the compound's binding to enzyme-substrate complex, most likely after the active site phosphorylation and targeting either E-P<sub>i</sub> or E·P<sub>i</sub>. This mode of inhibition was also observed for levamisole, theophylline and L-homoarginine and some inhibitors identified in the earlier rounds of screening.<sup>8,10</sup> Interestingly, all other series identified in the current HTS campaign demonstrated competitive inhibition with respect to the phosphate-donor substrate.<sup>11,12</sup> A similar study was performed to characterize the mode of TNAP inhibition by compound **1** with respect to the phosphate-acceptor substrate DEA. Compound **1** demonstrated noncompetitive inhibition against DEA (Figure 6B), and this is consistent with the activity profile of the sulfonamide series in the *in vitro* luminescent assay performed at different concentrations of DEA. This MOA indicates that the inhibitor could bind either before or after



DEA binding ( $E-P_i$  or  $E-P_i \cdot AOH$ ), suggesting that compound **1** occupies a distinct binding site. In contrast, the pyrazole series demonstrated competitive inhibition with respect to DEA, potentially occupying the site of DEA binding.<sup>12</sup>

## Conclusion

High-throughput screening utilizing luminescent and colorimetric assays led to the identification of several potent and selective, small molecule inhibitors of the TNAP enzyme. Hit validation and directed synthesis led to the establishment of **1** (2,5-dimethoxy-*N*-(quinolin-3-yl)benzenesulfonamide) as a potent TNAP inhibitor with excellent selectivity over other alkaline phosphatases, favorable ADME profiles, acceptable aqueous solubility, and good plasma levels after subcutaneous dosing. In addition, an equally potent inhibitor (119 nM) from this series, **18** (5-bromo-2-methoxy-*N*-(quinolin-3-yl)benzenesulfonamide), was also found through lead validation studies. These molecules may find utility to determine the potential of TNAP inhibitors as therapeutics for vascular calcification in target validation studies. Future work will describe the continued in vitro characterization and in vivo efficacy studies of this promising series of TNAP inhibitors.

## Experimental Section

**Compound Screening Library.** The compound library was supplied by the NIH Molecular Libraries Small Molecule Repository (MLSMR, <http://www.mli.nih.gov/mlsmr>). The MLSMR, funded by the NIH, is responsible for the selection of small molecules for HTS screening, their purchase and QC analysis, library maintenance, and distribution within the NIH Molecular Libraries Screening Center Network (MLSCN, <http://www.mli.nih.gov/mlscn>). Both MLSMR and MLSCN are components of the Molecular Libraries Initiatives (MLI, <http://nihroadmap.nih.gov/molecularlibraries>) within the NIH Roadmap Initiative ([www.nihroadmap.nih.gov](http://www.nihroadmap.nih.gov)). MLSMR compounds are acquired from commercial and, in part, from academic and government sources and are selected based on the following criteria: samples are available for resupply in 10 mg quantity, are at least 90% pure, have acceptable physicochemical properties, and contain no functional groups or moieties that are known to generate artifacts in HTS (<http://mlsmr.glp.com/>). Compounds are selected to represent diversified chemical space with clusters of closely related analogues to aid in the HTS-based SAR analysis.

**Expression and Preparation of Test Enzymes.** Expression plasmids containing a secreted epitope-tagged TNAP were transfected into COS-1 cells for transient expression.<sup>10</sup> The medium was replaced with Opti-MEM 24 h later, and the serum-free media containing secreted proteins were collected 60 h after electroporation. The conditioned medium was dialyzed against TBS containing 1 mM  $MgCl_2$  and 20 mM  $ZnCl_2$  (to remove phosphate) and filtered through a 0.22  $\mu m$  cellulose acetate filter.

**HTS Assays.** Assays were developed and performed as described in detail elsewhere.<sup>11</sup> Briefly, the TNAP luminescent assay was performed in 384-well white plates (784075, Greiner) at 50  $\mu M$  CDP-star substrate in assay buffer containing 100 mM DEA-HCl, pH 9.8, 1 mM  $MgCl_2$ , and 20  $\mu M$   $ZnCl_2$ . The luminescence signal was measured after a 30 min incubation at room temperature on an EnVision plate reader (Perkin-Elmer, Inc.). Analogous luminescent assays were optimized and utilized for PLAP and IAP with the CDP-star concentration adjusted to their respective  $K_m$  values, 85  $\mu M$  and 177  $\mu M$ , respectively.

The colorimetric TNAP assay was performed as previously described<sup>8</sup> with slight modifications. TNAP in assay buffer containing 1 M DEA-HCl, pH 9.8, 1 mM  $MgCl_2$ , and 20  $\mu M$   $ZnCl_2$  was added with 0.5 mM pNPP substrate, and after a 1 h

incubation, the reaction was terminated by adding 2,3-dimercapto-1-propanesulfonate (a compound that binds  $Zn^{2+}$  with high affinity thus inactivating the enzyme) to a concentration of 100  $\mu M$ . TNAP activity was measured using absorbance at 405 nm.

**General Synthetic Procedures.** All solvents and chemicals used were purchased from Sigma-Aldrich, Acros, or Chembridge and were used as received without further purification. Purity and characterization of compounds were established by a combination of liquid chromatography–mass spectroscopy (LC-MS) and NMR analytical techniques and was > 95% for all tested compounds. Silica gel column chromatography was carried out using prepacked silica cartridges from RediSep (ISCO Ltd.) and eluted using an Isco Companion system.  $^1H$  NMR spectra were acquired on a Varian Inova 300 MHz. Chemical shifts are reported in ppm from residual solvent peaks ( $\delta$  7.27 for  $CDCl_3$   $^1H$  NMR). High-resolution ESI-TOF mass spectra were acquired at the Center for Mass Spectrometry at The Scripps Research Institute (La Jolla, CA). HPLC-MS analyses were performed on a Shimadzu 2010EV LCMS using the following conditions: Kromasil C18 column (reverse phase, 4.6 mm  $\times$  50 mm); a linear gradient from 10% acetonitrile and 90% water to 95% acetonitrile and 5% water over 4.5 min; flow rate of 1 mL/min; UV photodiode array detection from 200 to 300 nm.

**General Method for the Synthesis of Sulfonamide TNAP Inhibitors.** To a stirred solution of the sulfonyl chloride (0.5 mmol in DMF), the appropriate aryl amine (0.5 mmol) was added, followed by *N,N*-diisopropylethylamine (0.75 mmol), and stirred at room temperature for 18 h. Solvents were removed by rotary evaporation, and the products were isolated by flash chromatography and reverse phase HPLC and lyophilized to provide the final compounds, which were determined to be > 95% pure by HPLC-UV, HPLC-MS, and  $^1H$  NMR.

**2,5-Dimethoxy-*N*-(quinolin-3-yl)benzenesulfonamide (1).** Prepared according to the general procedure to yield a yellow solid (67%).  $^1H$  NMR (300 MHz,  $CDCl_3$ ):  $\delta$  8.698 (s, 1H), 8.30 (d,  $J$  = 8.1 Hz, 1H), 8.10 (s, 1H), 8.01 (d,  $J$  = 7.8 Hz, 1H), 7.90 (t,  $J$  = 7.5 Hz, 1H), 7.79 (s, 1H), 7.42 (d,  $J$  = 2.7 Hz, 1H), 7.00 (m, 2H), 3.95 (s, 3H), 3.77 (s, 3H). ESI-MS  $m/z$  345  $[M + H]^+$ . HRMS  $m/z$  calcd for  $C_{17}H_{17}N_2O_4S$   $[M + H]^+$ : 345.0903. Found: 345.0903.

**2,5-Dimethoxy-*N*-(pyridin-3-yl)benzenesulfonamide (2).** Prepared according to the general procedure to yield a white solid (72%).  $^1H$  NMR (300 MHz,  $CDCl_3$ ):  $\delta$  9.01 (d,  $J$  = 2.4 Hz, 1H), 8.19 (m, 1H), 7.6 (m, 4H), 6.85 (m, 3H), 3.86 (s, 3H), 3.73 (s, 3H). ESI-MS  $m/z$  295  $[M + H]^+$ . HRMS  $m/z$  calcd for  $C_{13}H_{15}N_2O_4S$   $[M + H]^+$ : 295.0747. Found: 295.1435.

**2,5-Dimethoxy-*N*-(naphthalen-2-yl)benzenesulfonamide (12).** Prepared according to the general procedure to yield a white powder (6%).  $^1H$  NMR (300 MHz,  $CDCl_3$ ):  $\delta$  7.73 (m, 3H), 7.57 (d,  $J$  = 2.1 Hz, 1H), 7.42 (m, 4H), 7.29 (m, 1H), 6.98 (m, 2H), 4.05 (s, 3H), 3.72 (s, 3H). ESI-MS  $m/z$  344  $[M + H]^+$ . HRMS  $m/z$  calcd for  $C_{18}H_{18}NO_4S$   $[M + H]^+$ : 344.0951. Found: 344.0949.

**2,5-Dimethoxy-*N*-(quinolin-6-yl)benzenesulfonamide (13).** Prepared according to the general procedure to yield a yellow solid (35%).  $^1H$  NMR (300 MHz,  $CDCl_3$ ):  $\delta$  9.09 (s, 2H), 8.43 (d,  $J$  = 7.8 Hz, 1H), 8.30 (d,  $J$  = 8.1 Hz, 1H), 7.82 (d,  $J$  = 15.6 Hz, 3H), 7.44 (s, 1H), 7.0 (m, 2H), 3.93 (s, 3H), 3.75 (s, 3H). ESI-MS  $m/z$  345  $[M + H]^+$ . HRMS  $m/z$  calcd for  $C_{17}H_{17}N_2O_4S$   $[M + H]^+$ : 345.0903. Found: 345.0903.

**5-Chloro-2-methoxy-*N*-(quinolin-3-yl)benzenesulfonamide (14).** Prepared according to the general procedure to yield a yellow solid (17%).  $^1H$  NMR (300 MHz,  $DMSO-d_6$ ):  $\delta$  10.72 (s, 1H), 8.68 (s, 1H), 7.95 (m, 2H), 7.77 (m, 1H), 7.65 (m, 2H), 7.21 (d,  $J$  = 9.3 Hz, 1H), 3.85 (s, 3H). ESI-MS  $m/z$  349  $[M + H]^+$ . HRMS  $m/z$  calcd for  $C_{16}H_{14}ClN_2O_3S$   $[M + H]^+$ : 349.0408. Found: 349.0403.

**3-Methoxy-*N*-(quinolin-3-yl)benzenesulfonamide (15).** Prepared according to the general procedure to yield a yellow solid

(15%).  $^1\text{H}$  NMR (300 MHz, DMSO- $d_6$ ):  $\delta$  10.83 (s, 1H), 8.64 (d,  $J$  = 2.4 Hz, 1H), 8.03 (m, 1H), 7.94 (m, 2H), 7.65 (m, 2H), 7.45 (m, 1H), 7.35 (m, 1H), 7.17 (m, 1H), 3.75 (s, 3H). ESI-MS  $m/z$  315  $[\text{M} + \text{H}]^+$ . HRMS  $m/z$  calcd for  $\text{C}_{16}\text{H}_{15}\text{N}_2\text{O}_3\text{S}$   $[\text{M} + \text{H}]^+$ : 315.0798. Found: 315.0792.

***N*-(2,5-Dimethoxyphenyl)quinoline-3-sulfonamide (16).** To a stirred solution of the quinoline 3-sulfonyl chloride (0.5 mmol, 115 mg) in DMF, the 2,5-dimethoxy aniline (0.5 mmol, 76 mg) was added, followed by *N,N*-diisopropylethylamine (0.75 mmol). This mixture was stirred at room temperature overnight. Reverse phase HPLC afforded a white solid (7%).  $^1\text{H}$  NMR (300 MHz,  $\text{CDCl}_3$ ):  $\delta$  9.16 (d,  $J$  = 2.4 Hz, 1H), 8.60 (d,  $J$  = 2.4 Hz, 1H), 8.15 (m, 1H), 7.89 (m, 1H), 7.65 (m, 1H), 7.26 (d,  $J$  = 2.4 Hz, 2H), 7.19 (s, 1H), 6.60 (m, 2H), 3.79 (s, 3H), 3.52 (s, 3H). ESI-MS  $m/z$  345  $[\text{M} + \text{H}]^+$ . HRMS  $m/z$  calcd for  $\text{C}_{17}\text{H}_{17}\text{N}_2\text{O}_4\text{S}$   $[\text{M} + \text{H}]^+$ : 345.0903. Found: 345.0902.

**5-Bromo-2-methoxy-*N*-(quinolin-3-yl)benzenesulfonamide (18).** Prepared according to the general procedure to yield a white powder (36%).  $^1\text{H}$  NMR (300 MHz, DMSO- $d_6$ ):  $\delta$  10.71 (s, 1H), 8.69 (d,  $J$  = 3.0 Hz, 1H), 7.94 (m, 3H), 7.75 (m, 1H), 7.65 (m, 1H), 7.52 (m, 1H), 7.15 (d,  $J$  = 8.7 Hz, 1H), 3.85 (s, 3H). ESI-MS  $m/z$  394.8  $[\text{M} + \text{H}]^+$ . HRMS  $m/z$  calcd for  $\text{C}_{16}\text{H}_{14}\text{BrN}_2\text{O}_3\text{S}$   $[\text{M} + \text{H}]^+$ : 392.9903. Found: 392.9906.

**2-Methoxy-5-methyl-*N*-(quinolin-3-yl)benzenesulfonamide (19).** Prepared according to the general procedure to yield a yellow solid (3%).  $^1\text{H}$  NMR (300 MHz,  $\text{CDCl}_3$ ):  $\delta$  8.70 (s, 1H), 8.30 (d,  $J$  = 8.1 Hz, 1H), 8.01 (d,  $J$  = 7.8 Hz, 1H), 7.89 (m, 1H), 7.77 (m, 1H), 7.70 (s, 1H), 7.32 (m, 2H), 3.97 (s, 3H), 2.89 (s, 3H). ESI-MS  $m/z$  329  $[\text{M} + \text{H}]^+$ . HRMS  $m/z$  calcd for  $\text{C}_{17}\text{H}_{17}\text{N}_2\text{O}_3\text{S}$   $[\text{M} + \text{H}]^+$ : 329.0954. Found: 329.0960.

**2-Methoxy-4-nitro-*N*-(quinolin-3-yl)benzenesulfonamide (20).** Prepared according to the general procedure to yield a yellow powder (9%).  $^1\text{H}$  NMR (300 MHz, DMSO- $d_6$ ):  $\delta$  8.68 (d,  $J$  = 2.4 Hz, 1H), 8.10 (d,  $J$  = 8.4 Hz, 1H), 7.99 (d,  $J$  = 2.4 Hz, 1H), 7.92 (m, 3H), 7.84 (m, 1H), 7.65 (m, 1H), 7.55 (m, 1H), 3.99 (s, 3H). ESI-MS  $m/z$  360  $[\text{M} + \text{H}]^+$ . HRMS  $m/z$  calcd for  $\text{C}_{16}\text{H}_{14}\text{N}_3\text{O}_5\text{S}$   $[\text{M} + \text{H}]^+$ : 360.0649. Found: 360.0644.

**2-Methoxy-5-methyl-*N*-(pyridin-3-yl)benzenesulfonamide (21).** Prepared according to the general procedure to yield a yellow powder (43%).  $^1\text{H}$  NMR (300 MHz,  $\text{CDCl}_3$ ):  $\delta$  8.35 (m, 2H), 7.70 (m, 1H), 7.62 (s, 1H), 7.30 (m, 2H), 6.93 (m, 1H), 4.02 (s, 3H), 2.29 (s, 3H). ESI-MS  $m/z$  279  $[\text{M} + \text{H}]^+$ . HRMS  $m/z$  calcd for  $\text{C}_{13}\text{H}_{15}\text{N}_2\text{O}_3\text{S}$   $[\text{M} + \text{H}]^+$ : 279.0798. Found: 279.0801.

**2-Methoxy-4-nitro-*N*-(pyridin-3-yl)benzenesulfonamide (22).** Prepared according to the general procedure to yield a yellow solid (53%).  $^1\text{H}$  NMR (300 MHz,  $\text{CDCl}_3$ ):  $\delta$  8.73 (d,  $J$  = 4.8 Hz, 1H), 8.66 (s, 1H), 8.23 (m, 1H), 7.99 (m, 1H), 7.89 (s, 1H), 7.83 (m, 1H), 7.54 (m, 1H), 3.85 (s, 3H). ESI-MS  $m/z$  310  $[\text{M} + \text{H}]^+$ . HRMS  $m/z$  calcd for  $\text{C}_{12}\text{H}_{10}\text{N}_3\text{O}_5\text{S}$   $[\text{M} - \text{H}]^-$ : 308.0347. Found: 308.0347.

**Enzymatic Counterscreening Assays.** Phosphoethanolamine (PEA) activity for PHOSPHO1 was assayed discontinuously, at 37 °C, by measuring the amount of inorganic phosphate released, according to the previously described procedure,<sup>14</sup> adjusting the assay medium to a final volume of 0.15 mL. Standard conditions were 20 mM Tris buffer, pH 7.2, containing 25% glycerol (w/v), 25  $\mu\text{g/mL}$  BSA, 2 mM  $\text{MgCl}_2$ , and 2.5 mM PEA. The reaction was initiated by the addition of the enzyme and stopped with 0.075 mL of cold 30% TCA at appropriate time intervals. The reaction mixture was centrifuged at 4000g, and phosphate was quantified in the supernatant after pH neutralization with 0.1 M NaOH. *p*-Nitrophenylthymidine 5'-monophosphate (pNP-TMP) activity for NPP1 was assayed discontinuously, at 37 °C by following the liberation of *p*-nitrophenolate ion ( $\epsilon$  1 M, pH 13 = 17600  $\text{M}^{-1}\text{cm}^{-1}$ ) at 410 nm. Standard conditions were 50 mM Tris buffer, pH 7.4, or 100 mM Tris buffer, pH 8.9, containing 2 mM  $\text{MgCl}_2$  and 5 mM pNP-TMP, in a final volume of 0.15 mL. The reaction was initiated by the addition of the enzyme and stopped with 0.15 mL of 1 M NaOH at appropriate time intervals. All

determinations were carried out in triplicate, and the initial velocities were constant for at least 90 min, provided that less than 5% of substrate was hydrolyzed. Controls without added enzyme were included in each experiment to allow for the nonenzymatic hydrolysis of substrate. We used the inhibitor compound **1** at a final concentration of 10  $\mu\text{M}$  to assess its effect on PHOSPHO1 and NPP1 activities.

**Assessment of Plasma and Microsomal Stability and Permeability.** To assess plasma stability, the test compounds were incubated in fresh rat plasma at 37 °C. To determine metabolic stability, the compounds in triplicate were incubated with pooled rat liver microsomes (BD Scientific) in the presence of NADPH (Sigma) at 37 °C. Liquid chromatography/mass spectrometry (LC/MS) was applied in quantitative analysis of compounds in the biological matrix. Mass spectrometry (Shimadzu 2010EV) was used to conduct mass analysis in multiple-reaction-monitoring (MRM) mode. The compound stabilities, expressed as the percentage of the remaining compound to the initial concentration, were calculated using Shimadzu LabSolutions software and Excel. The permeability was determined using the PAMPA method described previously.<sup>15</sup>

**Solubility.** Solubility analysis was performed using a direct UV kinetic solubility method in a 96-well plate format. All liquid dispense and transfer steps were performed with the Freedom Evo automated liquid handler (Tecan US). Solubility measurements were performed in an aqueous buffer solution (System Solution, pION Inc.) at pH 7.4 in duplicate. Samples were incubated at room temperature for a minimum of 18 h to achieve equilibrium and then filtered (filter plate, pION Inc.) to remove any precipitate formed. The concentration of the compounds was measured by UV absorbance (250–498 nm) using the Infinite M200 (Tecan US) and compared to the spectra of the precipitation-free reference solutions. Spectroscopically pure 1-propanol (Sigma) was used as a cosolvent to suppress precipitation in the reference solutions. The solubility of each compound was determined using  $\mu\text{SOL}$  Evolution Plus software v3.2 (pION Inc.) and is expressed as the concentration ( $\mu\text{g/mL}$ ) of a solute in a saturated solution.

**Plasma Concentration Analysis.** For evaluation of in vivo compound concentration, 400  $\mu\text{L}$  of a 10  $\mu\text{M}$  solution of **1** (4.13 mg/kg; 50% DMSO in normal saline) were subcutaneously injected in each rat. Blood samples were drawn and frozen immediately. Plasma was harvested and kept at –20 °C until assayed. Concentrations of **1** in plasma were determined using a validated analytical procedure based on high-performance liquid chromatography. LC-MS/MS analyses were carried out using a SCIEX API3000 triple quadrupole mass spectrometer (PE Sciex Instruments, Boston, MA) operating in electrospray ionization mode. Chromatography was carried out using gradient elution (water–acetonitrile) on a Kromisil C18 reverse-phase column at a flow rate of 1 mL/min. Plasma compound concentrations were determined using a seven-point calibration curve derived from peak areas obtained from serially diluted solutions of **1**.

**Acknowledgment.** This work was supported in part by NIH grants U54HG003916, DE12889, AR47908, AR53102 and HL101899.

## References

- (1) Millán, J. L. *Mammalian Alkaline Phosphatases: From Biology to Applications in Medicine and Biotechnology*; Wiley-VCH Verlag GmbH & Co: Weinheim, Germany, 2006; 322 pp.
- (2) Hesse, L.; Johnson, K. A.; Anderson, H. C.; Narisawa, S.; Sali, A.; Goding, J. W.; Terkeltaub, R.; Millán, J. L. Tissue-nonspecific alkaline phosphatase and plasma cell membrane glycoprotein-1 are central antagonistic regulators of bone mineralization. *Proc. Natl. Acad. Sci. U.S.A.* **2002**, *99*, 9445–9449.
- (3) Harmey, D.; Hesse, L.; Narisawa, S.; Johnson, K. A.; Terkeltaub, R.; Millán, J. L. Concerted regulation of inorganic pyrophosphate

- and osteopontin by Akp2, Enpp1 and Ank: an integrated model of the pathogenesis of mineralization disorders. *Am. J. Pathol.* **2004**, *164*, 1199–1209.
- (4) Addison, W. N.; Azari, F.; Sørensen, E. S.; Kaartinen, M. T.; McKee, M. D. Pyrophosphate inhibits mineralization of osteoblast cultures by binding to mineral, up-regulating osteopontin, and inhibiting alkaline phosphatase activity. *J. Biol. Chem.* **2007**, *282*, 15872–15873.
- (5) Murshed, M.; Harmey, D.; Millán, J. L.; McKee, M. D.; Karsenty, G. Unique coexpression in osteoblasts of broadly expressed genes accounts for the spatial restriction of ECM mineralization to bone. *Genes Dev.* **2005**, *19*, 1093–1104.
- (6) Terkeltaub, R. A. Inorganic pyrophosphate generation and disposition in pathophysiology. *Am. J. Physiol. Cell Physiol.* **2001**, *281*, C1–C11.
- (7) Jono, S.; Shioi, A.; Ikari, Y.; Nishizawa, Y. Vascular calcification in chronic kidney disease. *J. Bone Miner. Metab.* **2006**, *24*, 176–181.
- (8) Narisawa, S.; Harmey, D.; Yadav, M. C.; O'Neill, W. C.; Hoylaerts, M. F.; Millán, J. L. Novel inhibitors of alkaline phosphatase suppress vascular smooth muscle cell calcification. *J. Bone Miner. Res.* **2007**, *22*, 1700–1710.
- (9) Lomashvili, K. A.; Garg, P.; Narisawa, S.; Millán, J. L.; O'Neill, W. C. Upregulation of alkaline phosphatase and pyrophosphate hydrolysis: Potential mechanism for uremic vascular calcification. *Kidney Int.* **2008**, *73*, 1024–1030.
- (10) Kozlenkov, A.; Hoylaerts, M. F.; Ny, T.; Le Du, M.; Millán, J. L. Residues determining the binding specificity of uncompetitive inhibitors to tissue-nonspecific alkaline phosphatase. *J. Bone Miner. Res.* **2004**, *19*, 1862–1872.
- (11) Sergienko, E.; Su, Y.; Chan, X.; Brown, B.; Hurder, A.; Narisawa, S.; Millán, J. L. Identification and Characterization of Novel Tissue-Nonspecific Alkaline Phosphatase Inhibitors with Diverse Modes of Action. *J. Biomol. Screen.* **2009**, *14*, 824–837.
- (12) Siddique, S.; Ardecky, R.; Su, Y.; Narisawa, S.; Brown, B.; Millán, J. L.; Sergienko, E.; Cosford, N. D. Design and synthesis of pyrazole derivatives as potent and selective inhibitors of tissue-nonspecific alkaline phosphatase (TNAP). *Bioorg. Med. Chem. Lett.* **2009**, *19*, 222–225.
- (13) Roberts, S.; Narisawa, S.; Harmey, D.; Millán, J. L.; Farquharson, C. Functional involvement of PHOSPHO1 in matrix vesicle-mediated skeletal mineralization. *J. Bone Miner. Res.* **2007**, *22*, 617–627.
- (14) Pizauro, J. M.; Ciancaglini, P.; Leone, F. A. Characterization of the phosphatidylinositol-specific phospholipase C-released form of rat osseous plate alkaline phosphatase and its possible significance on endochondral ossification. *Mol. Cell. Biochem.* **1995**, *152*, 121–129.
- (15) Kansy, M.; Senner, F.; Gubernator, K. Physicochemical High Throughput Screening: Parallel Artificial Membrane Permeation Assay in the Description of Passive Absorption Processes. *J. Med. Chem.* **1998**, *41*, 1007–1010.